Journal of Power Sources 196 (2011) 10344–10350

Contents lists available at SciVerse ScienceDirect

Journal of Power Sources

journal homepage: www.elsevier.com/locate/jpowsour

Electrochemistry and safety of $Li_4Ti_5O_{12}$ and graphite anodes paired with $LiMn_2O_4$ for hybrid electric vehicle Li-ion battery applications☆

Ilias Belharouak*, Gary M. Koenig Jr., K. Amine

Argonne National Laboratory, Chemical sciences and Engineering Division, 9700 S. Cass Ave., Argonne, IL 60439, USA

ARTICLE INFO

Article history:
Received 7 July 2011
Received in revised form 17 August 2011
Accepted 18 August 2011
Available online 25 August 2011

Keywords:
HEV
PHEV
Lithium battery
Lithium Titanate
Spinel
Safety

ABSTRACT

A promising anode material for hybrid electric vehicles (HEVs) is $Li_4Ti_5O_{12}$ (LTO). LTO intercalates lithium at a voltage of ~1.5 V relative to lithium metal, and thus this material has a lower energy compared to a graphite anode for a given cathode material. However, LTO has promising safety and cycle life characteristics relative to graphite anodes. Herein, we describe electrochemical and safety characterizations of LTO and graphite anodes paired with $LiMn_2O_4$ cathodes in pouch cells. The LTO anode outperformed graphite with regards to capacity retention on extended cycling, pulsing impedance, and calendar life and was found to be more stable to thermal abuse from analysis of gases generated at elevated temperatures and calorimetric data. The safety, calendar life, and pulsing performance of LTO make it an attractive alternative to graphite for high power automotive applications, in particular when paired with $LiMn_2O_4$ cathode materials.

1. Introduction

After the successful of introduction of nickel–metal hydride batteries into a variety of automotives, increased research is being performed towards the next generation of batteries for transportation, which will likely be partially or fully powered by lithium-ion batteries [1]. Lithium-ion batteries offer the advantages of having greater capacity and increased continuous and pulsed power relative to nickel–metal hydride batteries, which results in smaller and lighter batteries [2]. However, there are still a number of challenges in using lithium-ion batteries for large-scale applications such as hybrid electric vehicles (HEVs) and plug-in hybrid electric vehicles (PHEVs). These barriers include the calendar life (15 years), cost ($20 per kW HEV, $300 per kWh PHEV), and safety. Among the cell chemistries that have the potential to overcome these challenges, the $Li_4Ti_5O_{12}/LiMn_2O_4$ (noted in the text as LTO/LMO) system has been proposed as a cell chemistry that would be very attractive for lithium-ion batteries used in HEVs [3,4].

Pairing of LTO (also written as $Li[Li_{1/3}Ti_{5/3}]O_4$) as an anode with a LMO spinel cathode in a lithium-ion cell was first demonstrated by Thackeray et al. [5,6] in the mid-nineties. Some of the earliest investigations of LTO-type materials were over fifty years ago, when Durif et al. [7] investigated the synthesis of new types of materials derivatives of the spinel material Al_2MgO_4 and reported the first crystal structure of lithium and titanium-based oxides. Their crystallographic study was not able to distinguish between ($5TiO_2$, $2Li_2O$) and ($7TiO_2$, $2Li_2O$) as the two possible chemical compositions of these new compounds, although they were able to determine the cubic parameters (8.35 Å) of the unit cell and locate the lithium ions at the tetrahedral sites 8(a) of the spinel structure. Twenty years later, Deschanvres et al. [8] reported the full structure of LTO ($5TiO_2$, $2Li_2O$): they located the lithium ions at the tetrahedral (8a) sites, the remaining lithium ions and the tetravalent titanium ions at the (16d) sites, and the oxygen ions at the (32e) sites. In the late seventies, the demand for high energy density batteries stimulated the discovery of the Li/TiS_2 rechargeable lithium battery [9], and subsequently $LiTi_2O_4$ and LTO materials were found to reversibly react with lithium at room temperature [10]. In the late eighties, Dahn et al. [11,12] reported the first electrochemical study of the Li/LTO cell where a plateau voltage at 1.56 V was attributed to the insertion of one lithium ion into the structure of LTO. Thereafter, Ohzuku et al. [13,14] reported the first comprehensive electrochemical and structural study of LTO. In these studies, the authors introduced LTO spinel as a zero-strain lithium insertion material since the lattice parameters do not change during the insertion/extraction of lithium ions into/out of the material.

☆ The submitted manuscript has been created by UChicago Argonne, LLC, Operator of Argonne National Laboratory ("Argonne"). Argonne, a U.S. Department of Energy Office of Science laboratory, is operated under Contract No. DE-AC02-06CH11357. The U.S. Government retains for itself, and others acting on its behalf, a paid-up nonexclusive, irrevocable worldwide license in said article to reproduce, prepare derivative works, distribute copies to the public, and perform publicly and display publicly, by or on behalf of the Government.

* Corresponding author. Tel.: +1 630 252 4450; fax: +1 630 252 4671.
E-mail address: belharouak@anl.gov (I. Belharouak).

0378-7753/$ – see front matter © 2011 Elsevier B.V. All rights reserved.
doi:10.1016/j.jpowsour.2011.08.079

Structurally, the lithium insertion into LTO spinel results in the displacement of the lithium ions originally located at the tetrahedral site 8(a) into the octahedral 16(c) sites that also accommodates the newly inserted lithium ions according to the following scheme:

$$Li_{1,8(a)}\,[Li_{1/3}Ti_{5/3}]_{,16(d)}O_4(\text{spinel}) + 1\ Li^+ \rightleftarrows Li_{2,16(c)}[Li_{1/3}Ti_{5/3}]_{16(d)}\,O_4(\text{rock-salt})$$

This electrochemical reaction suggests the formation of a rock-salt compound $Li_2\ [Li_{1/3}Ti_{5/3}]O_4$ (or $Li_7Ti_5O_{12}$) and generates 175 mA h g^{-1} theoretical capacity at full lithiation. This two-phase reaction takes place at a flat voltage of 1.5 V vs. Li in an electrode during the lithium insertion reaction [15–20].

In contrast to conventional graphite anodes, no volume change is expected during the insertion of lithium atoms in the spinel structure of LTO, leading to the formation of a rock-salt type $Li_7Ti_5O_{12}$ material with a zero-strain structural character. When coupled with a 4-V cathode material, such as the three dimensional LMO spinel [5,6], the cell provides a 2.5 V operating voltage, twice the voltage of a nickel–metal hydride cell. Replacement of graphite by LTO in a lithium-ion battery will result in a reduction in the operating cell voltage, which reduces the overall energy density at the cell level. The loss in energy density due to the absence of graphite must be weighed against the improvements in intrinsic cycle-life and safety that using a LTO anode may provide, and in addition the LTO/LMO chemistry may be attractive for high power battery applications which is supported by the results demonstrated in this manuscript [4]. It has been reported that the lifetime of the graphite/$LiMn_2O_4$ (G/LMO) cell chemistry is dramatically shortened because manganese ions from the cathode dissolved into the electrolyte and poisoned the SEI layer, which is indispensable for shuttling lithium ions in and out of the graphite [21]. In this paper, we report on the cycle life and safety of LTO/LMO cells as compared to G/LMO cells, when cycled and evaluated at the level of 10 mA h pouch cells.

2. Experimental

LTO spinel was prepared by reacting stoichiometric amounts of Li_2CO_3 and TiO_2 (Rutile, 1–5 μm powder) at 850 °C for 24 h. LMO spinel was prepared by a solid-state reaction that consisted of mixing Li_2CO_3 and $MnCO_3$ precursors and heating the mix for 24 h at 850 °C. Spherical $MnCO_3$ precursor was initially synthesized by co-precipitation from an aqueous solution containing manganese sulfate by the addition of a second aqueous solution containing Na_2CO_3 and NH_4OH according to the procedure detailed previously [22].

Powder X-ray diffraction (XRD) patterns of the samples were recorded on a Siemens D5000 powder diffractometer, using CuKα radiation in the angular range of 10–80° (2θ) with a 0.02° (2θ) step.

Scanning electron microscopy images were taken at the Electron Microscopy Center (EMC) at Argonne National Laboratory using a field-emission scanning electron microscope (Hitachi S-4700-II).

Positive electrodes were made by coating an aluminum foil collector with a paste comprised of LMO active material, carbon black (as a conducting additive), and polyvinylidene fluoride (PVdF) binder (in the proportions 80:10:10 wt%). The negative electrode was prepared by mixing LTO with 10-wt% carbon and 10-wt% PVdF binder; and a copper foil was coated with the resulting paste. Both positive and negative electrodes were ~40–50 μm thick, and assembled cells were slightly cathode limited. The electrolyte was 1.2-M $LiPF_6$ in a 30:70 wt% mixture of ethyl carbonate (EC) and ethyl methyl carbonate (EMC). The cells, assembled inside a helium-filled dry-box, were evaluated using pouch-type cells. The charge/discharge measurements were carried out over a potential range between 1.5 and 3.0 V. For charge/discharge cycling, a current of 100 mA g^{-1} was used as 1C and was based on the cathode (LMO) mass.

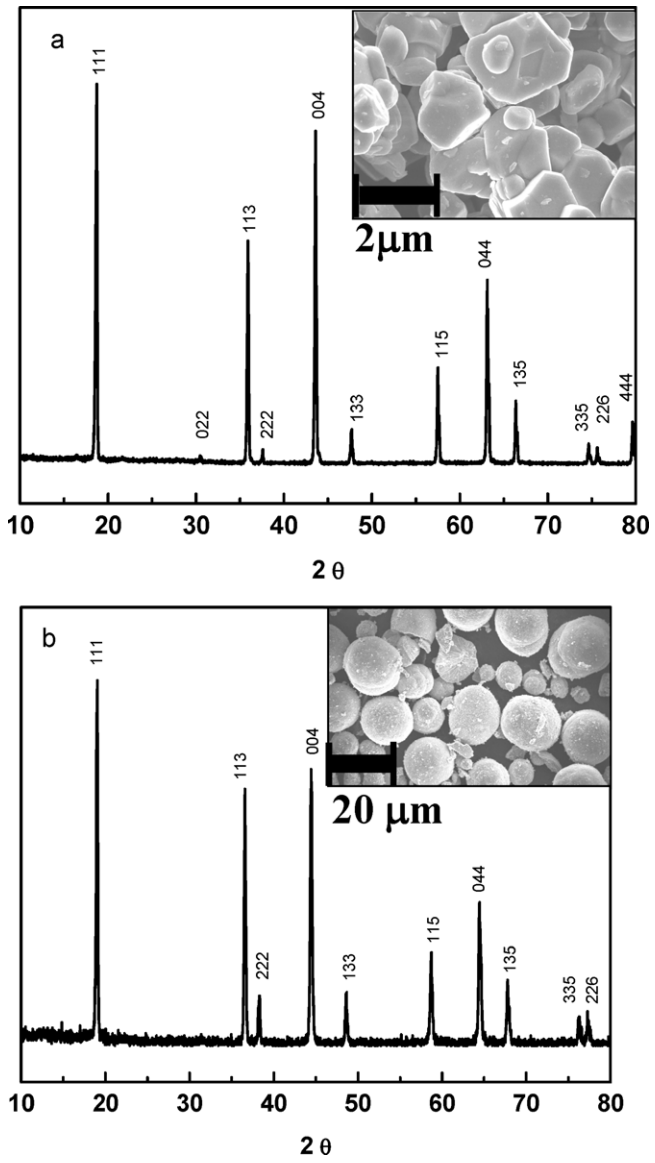

Fig. 1. X-ray diffraction patterns and scanning electron micrographs (inserts) for the prepared (a) $Li_4Ti_5O_{12}$ (LTO) and (b) $LiMn_2O_4$ (LMO).

Differential scanning calorimetry (DSC) experiments were conducted using a Perkin-Elmer Pyris 1 instrument, on electrochemically delithiated cathodes (LMO) and lithiated anodes (graphite or LTO). Typically, 3 mg of material and 3 μL of electrolyte were hermetically sealed inside stainless-steel high-pressure capsules to prevent leakage of pressurized solvents. The DSC curves were recorded between room temperature and 375 °C at a scan rate of 10 °C min^{-1}. An empty stainless-steel capsule was used as a reference pan. Gas chromatography (GC) and mass spectrometry (MS) were done using a Hewlett–Packard integrated GC–MS system. The GC–MS was calibrated with standard gases that were used to determine retention times.

3. Results and discussion

Fig. 1 shows the XRD patterns of the LTO (Fig. 1a) and LMO (Fig. 1b) pristine materials. In both cases, the observed diffraction

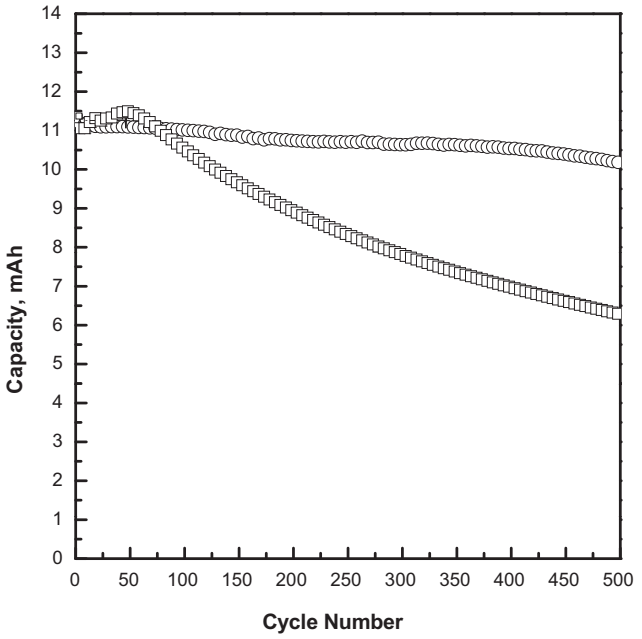

Fig. 2. Cell discharge capacity during 500 charge/discharge cycles for LTO/LMO (circles) and G/LMO (squares) pouch cells cycled at 6C charge and discharge rates at a temperature of 55 °C.

lines can be indexed based on the Fd-3m space group. The cubic lattice parameters are 8.358 and 8.245 Å for LTO and LMO, respectively. These values are consistent with findings in several reports [8,14,23]. The morphologies and particle sizes of the LTO and LMO materials are shown in the inserts of Fig. 1. LTO consisted of particles with diameters primarily in the range of 2–3 μm, but larger particles were observed as a result of agglomeration. The LMO consisted of approximately spherical particles with diameters varying between 10 and 20 μm.

As mentioned above, the lifetime of a battery with the G/LMO cell chemistry is severely shortened at elevated temperatures. This problem is a major challenge in using this cathode in large scale commercial Li-ion batteries despite its high power capability and reasonable energy density [21]. Approaches to avoid the capacity fade of G/LMO batteries include developing new electrolytes [20] and electrolyte additives [24], and additional engineering of the battery pack to provide heat exchangers and temperature regulation of the battery. These two approaches can add cost and weight to the battery pack. Another alternative approach is to replace the graphite with an anode that can better tolerate elevated temperatures, such as LTO. To demonstrate this approach, two Li-ion cells were designed with G/LMO and LTO/LMO, both having the same electrolyte and approximately the same initial capacities. After assembly, the cells were stored at 55 °C and subjected to a continuous 6C rate of charge and discharge. After 500 cycles, the cell comprising LTO exhibited a 10% capacity loss, while the cell made with a graphite anode lost more than 40% of its initial capacity (Fig. 2). Analysis by inductively coupled plasma of the electrolytes recovered from both cells confirmed the existence of Mn^{2+} ions in the solution. However, the impact of Mn^{2+} ions dissolved into the electrolyte on the capacity of the cells was much more pronounced for the graphite anode because of the poisoning effect of the solid electrolyte interface (SEI) layer formed at the graphite surface. In a previous report [21], it was found that a few ppm of Mn^{2+} ions can cause a major modification of the characteristics of the SEI layer, leading to cell failure after a continuous rise in interfacial impedance at the graphite negative electrode. To stabilize the G/LMO cell chemistry at elevated temperature, work has been done

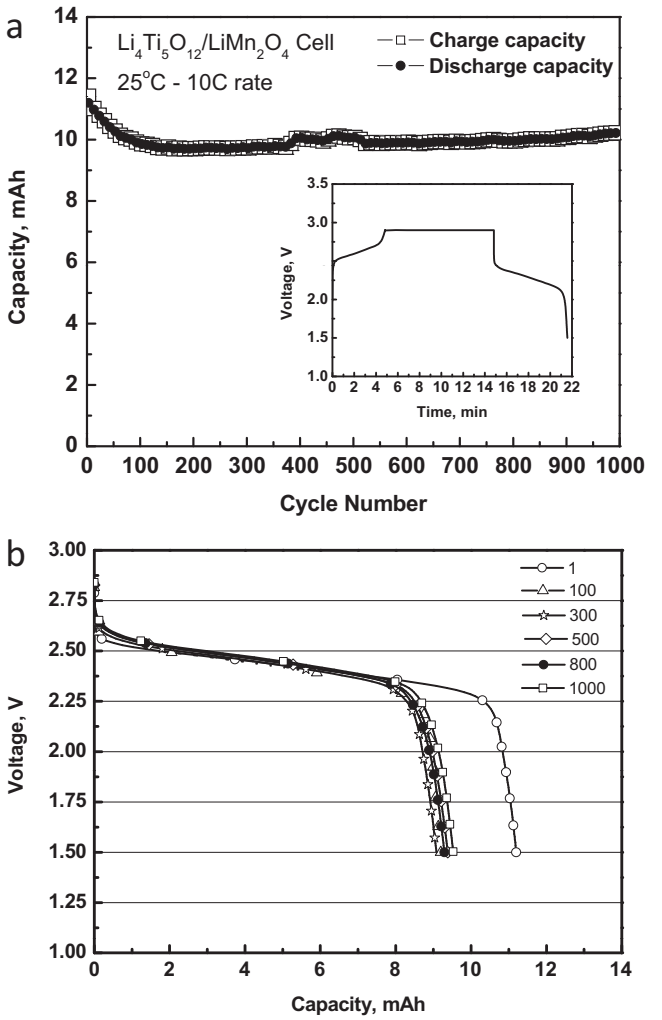

Fig. 3. (a) LTO/LMO cell discharge capacity during 1000 charge/discharge cycles at 10C rate of charge and discharge at 25 °C. The insert shows the voltage as a function of time during the first charge/discharge cycle. (b) Discharge profiles for selected cycles of the LTO/LMO cell.

with the aim of preventing or reducing manganese dissolution via the replacement the $LiPF_6$ salt with other salts that do not generate HF acid [20], coating LMO with metal oxides such as zinc oxide [19], or stabilizing the SEI layer with additives [24]. With respect to these approaches, another way to get full usage of the power and safety characteristics of LMO is by replacing graphite by an alternative anode, in this case LTO, which does not require a SEI layer.

HEV applications require rather high-power density batteries, because the available energy (300 Wh) over the depth of discharge range where the power goals are met is only a fraction of the total energy that the fully depleted battery can provide. To demonstrate that the LTO/LMO battery retains capacity at higher rates which would be more relevant for the high power requirements of HEV batteries, we further confirmed the retention of capacity of LTO/LMO cells by cycling pouch cells with ~10 mA h capacities at a higher rate (10C, at both 25 °C and 55 °C). The pouch cells cycled at 10C retained 89.3% and 92.7% of their initial capacity after 1000 cycles at 25 °C (Fig. 3) and 55 °C (Fig. 4), with the majority of the capacity loss occurring during the first 100 cycles. From 100 to 1000 cycles, there also is minimal voltage depression, which means that both the capacity and deliverable energy of the cells was retained well during 1000 charge/discharge cycles.

In addition to tolerating high rates to provide power over many cycles, HEV batteries need significant pulsing capabilities.

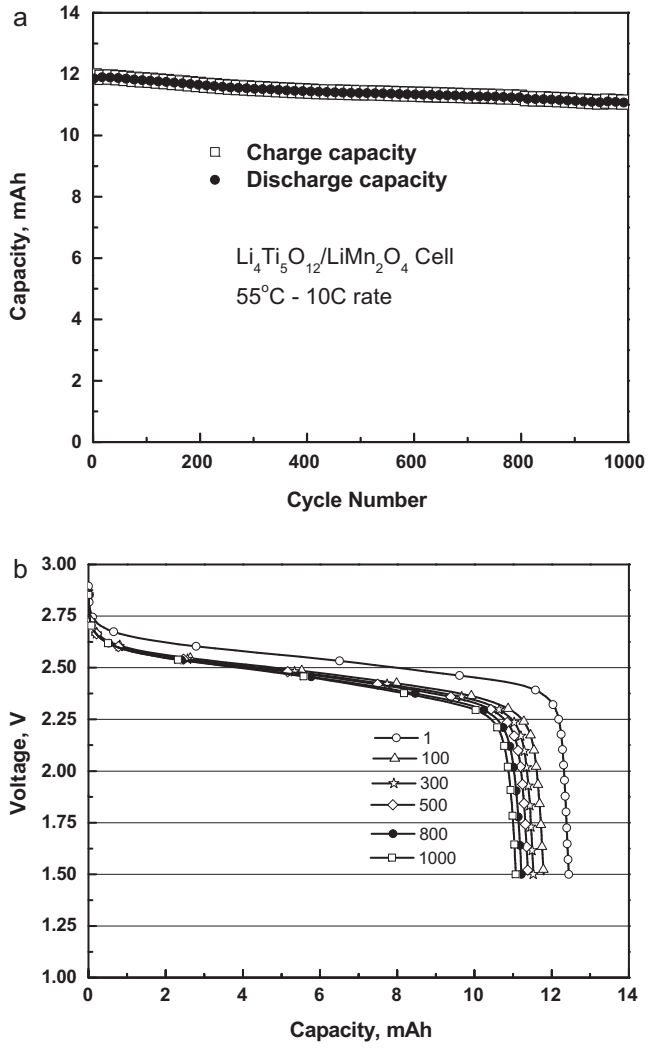

Fig. 4. (a) LTO/LMO cell discharge capacity during 1000 charge/discharge cycles at 10C rate of charge and discharge at 55 °C. (b) Discharge profiles for selected cycles of the LTO/LMO cell.

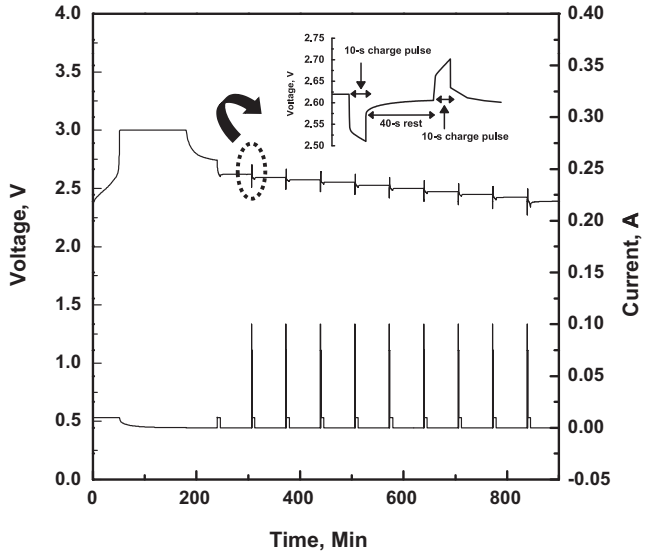

Fig. 5. Voltage and current as a function of time during a hybrid pulsed power characterization (HPPC) test of LTO/LMO cell. Insert shows individual pulse profile.

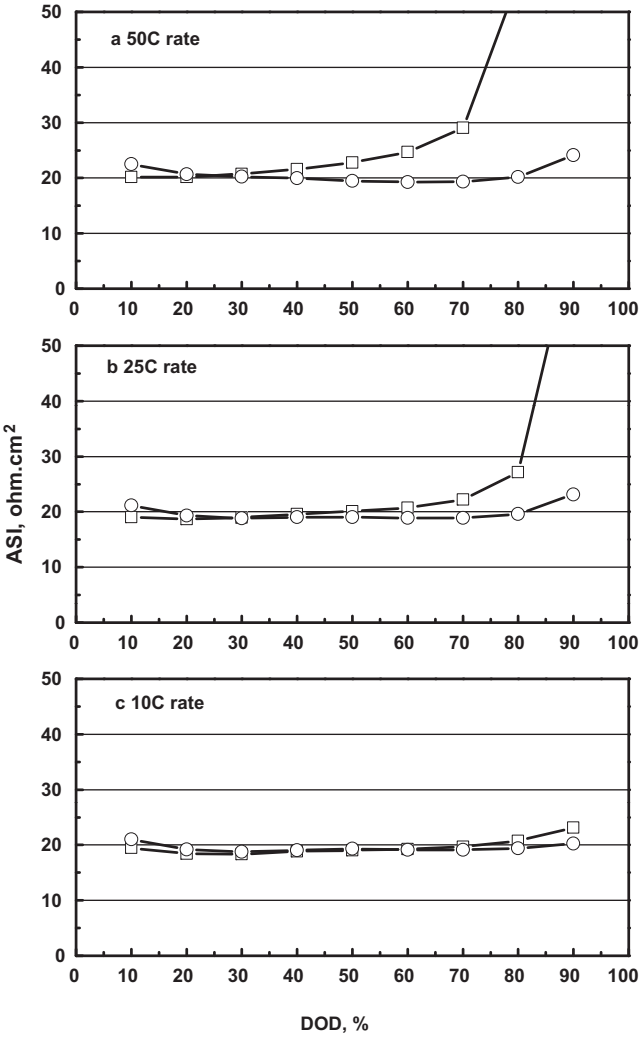

Fig. 6. Area specific impedance (ASI) at the full range of depths of discharge (DOD) during HPPC testing on a LTO/LMO cell at discharge (circles)/charge (squares) pulses of (a) 50C/37.5C, (b) 25C/18.75C, and (c) 10C/7.5C.

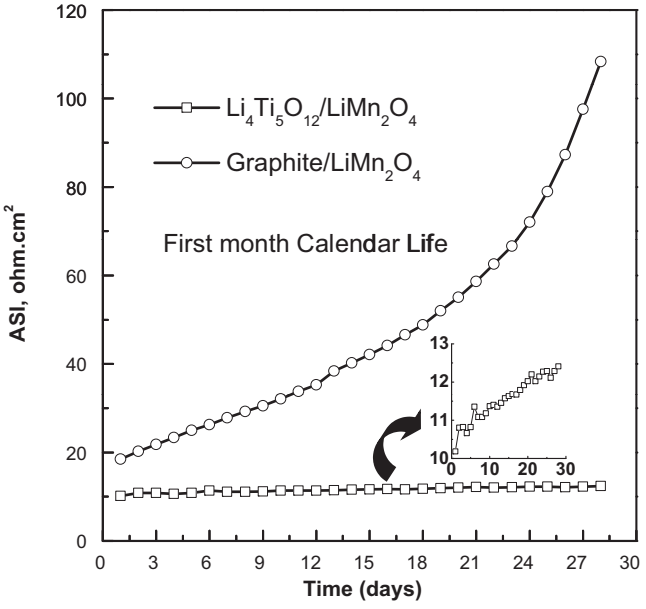

Fig. 7. ASI measured over 28 days for LTO/LMO (squares) and G/LMO (circles).

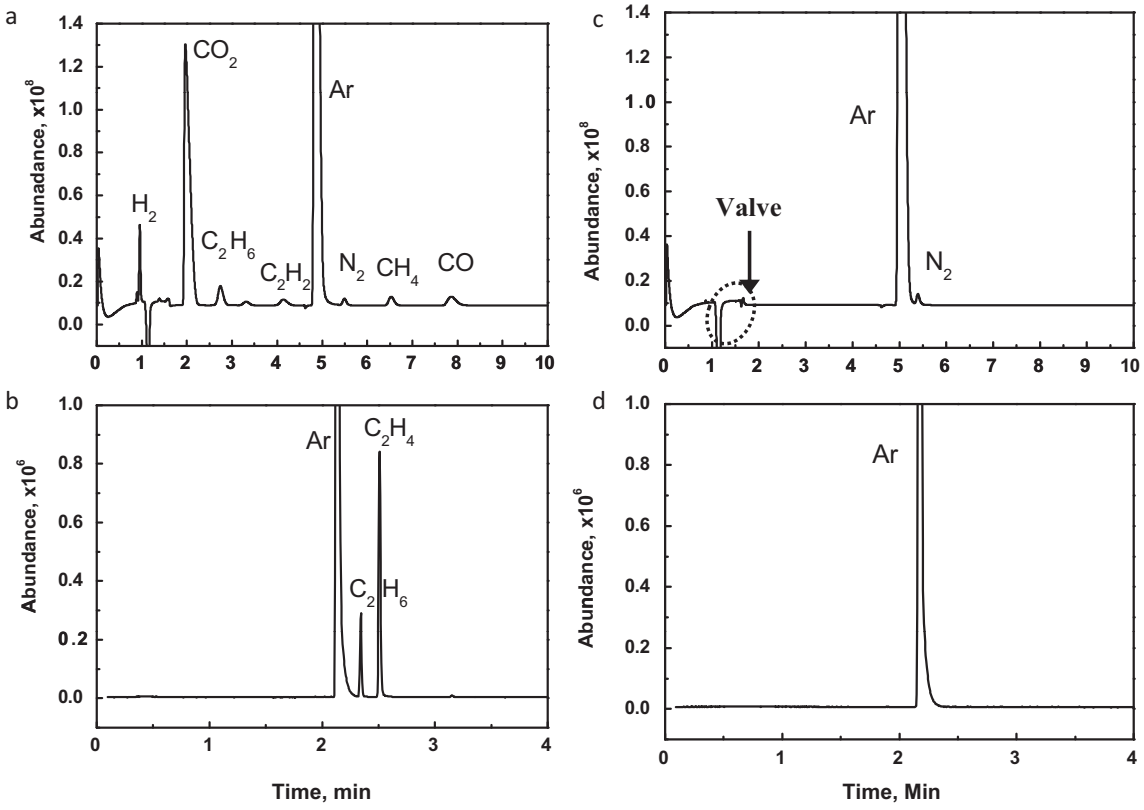

Fig. 8. Gas chromatography (GC) and mass spectrometry (MS) from gas collected from Li/G and Li/LTO pouch cells discharged to 1.0 mV and 1.0 V, respectively, and then held at 100 °C for 12 h. (a) GC of G/LMO, (b) MS of G/LMO, (c) GC of LTO/LMO, and (d) MS of LTO/LMO.

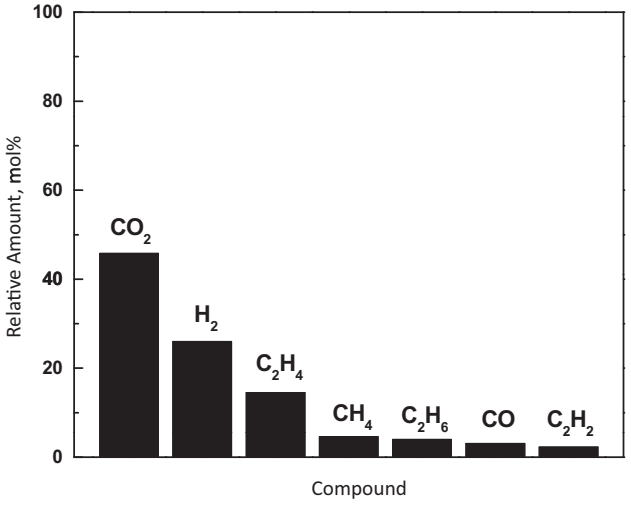

Fig. 9. Relative quantities of gases collected from G/Li cell as determined by GC, excluding Ar gas.

We performed hybrid pulsed power characterization (HPPC) on our materials to determine their performance during pulsing at different states of charge. A typical HPPC test profile is shown in Fig. 5. During the HPPC test, the pouch cell was charged to full capacity (3.0 V). Then, 10% of the capacity was discharged at a 1C rate. After a 1 h rest period, the cell was discharged for a 10 s pulse, allowed to rest for 40 s, charged for a 10 s pulse (at 75% of the discharge rate), and discharged at 1C until an additional 10% of the capacity had been discharged. The pulsing procedure was repeated at each 10% increment of the state of charge for the cell. The area specific impedance (ASI) during charge and discharge at discharging rates of 50C, 25C, and 10C (charging rates of 37.5, 18.75, and 7.5C) at different depths of discharge calculated from the HPPC tests can be found in Fig. 6. A typical upper acceptable limit for ASI values during pulsing is 35 Ω cm^2 [25], and these LTO/LMO pouch cells are below this ASI for every depth of discharge at the 10C/7.5C pulses (Fig. 6a), and exceed 35 Ω cm^2 only during charging at 90% and above 80% depth of discharge at 25C/18.75C and 50C/37.5C rates, respectively. The low ASI values for realistic pulsing conditions (up to 50C) across most of the depths of discharge (at least up to 70%) indicates that the LTO/LMO material has promise as a full cell material for applications that require high pulse rates, such as HEVs and PHEVs. To further investigate the potential of this material, we performed calendar life and safety studies on this battery chemistry, and again compared the LTO/LMO chemistry to a conventional LMO cathode paired with graphite (G/LMO).

The results of calendar life testing for LTO/LMO and G/LMO can be seen in Fig. 7. Calendar life testing was done by charging the cells to 70% state of charge and holding at that voltage. Once per day for 28 days the cell was pulsed with a 5C discharge for 10 s followed by a 40 s rest and then a 10 s charge at 3.75C. The cell was then brought back up to the voltage at 70% state of charge and held there until the pulse the next day. This testing was performed at 55 °C. The ASI values shown in Fig. 7 were calculated from the discharge pulses. The ASI for the LTO/LMO battery gradually increased over the 28 days from 10.2 to 12.4 Ω cm^2. In contrast, the G/LMO battery had a huge increase in ASI over the same time period, from 18.5 to 108.3 Ω cm^2. LMO cathode materials are known to undergo Mn dissolution into the electrolyte, especially during cycling at elevated temperatures [21]. While the Mn will dissolve from the cathode in both cells, the cell with a graphite anode discharges to a lower potential and requires a stable SEI layer to cycle effectively. Previous studies have demonstrated that the dissolved Mn can migrate across the battery to the anode and disrupt the SEI layer, resulting in decreased

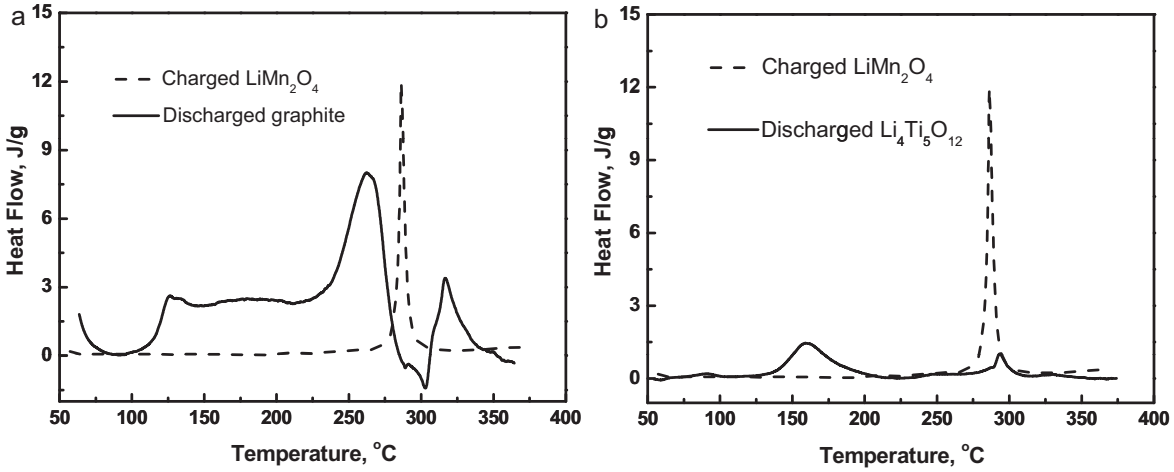

Fig. 10. Differential scanning calorimetry (DSC) run on the cathode and anode harvested from fully charged (a) G/LMO and (b) LTO/LMO cells.

capacity and increased impedance [21]. LTO operates at higher voltages compared to graphite that are stable when in contact with the electrolyte and do not require graphitic-SEI formation. The significantly lower ASI values after 28 days for the LTO/LMO cell compared to the G/LMO demonstrates that the LTO has much better calendar life properties, likely because it does not require SEI formation.

Safety is a major consideration for batteries in automotive applications. We next performed analysis of gases generated by graphite and LTO Li half cells, as well as differential scanning calorimetry (DSC) on full cells paired with LMO, to compare the safety characteristics between the two anode chemistries. First, we assembled Li half cell pouch cells with graphite and LTO. The graphite cell was discharged to 1 mV and the LTO cell was discharged to 1.0 V. Both cells were then heated to 100 °C in an oven and held at this elevated temperature for 12 h. After removing the cells from the oven they were taken into an Ar-filled glove box and a syringe was inserted into the pouch to extract any gases that may have been generated inside the cells. The gas extracted into the syringe was then analyzed using gas chromatography (GC) and mass spectrometry (MS). The GC and MS were both calibrated using the same standard gases. The GC and MS for the gases collected from both cells can be seen in Fig. 8. All data sets have a pronounced peak from Ar gas, which we attribute to the Ar atmosphere from the glove box. The GC and MS do not indicate any decomposition products for the LTO cell, and other than the pronounced Ar peak from the glove box atmosphere, only a small N_2 peak is even discernable. In contrast, a variety of gases were detected for the sample taken from the graphite cell. The GC indicates the presence of H_2, CO_2, C_2H_6, C_2H_2, N_2, CH_4, and CO and the MS has large C_2H_6 and C_2H_4 peaks. The various carbonaceous gaseous species indicate decomposition of the graphite SEI during the prolonged exposure to a 100 °C temperature. The relative abundance of these gases is shown in Fig. 9. The generation of these flammable gaseous species is a serious safety concern for graphite anodes. In contrast, the fully lithiated LTO did not generate any gaseous decomposition products. The stability of the LTO spinel structure coupled with the lack of a SEI makes this material more stable against forming gaseous degradation products at elevated temperatures compared to graphite [26].

While the LTO did not generate any gaseous degradation products during prolonged exposure to 100 °C, we also performed DSC on both cathode and anode materials up to 375 °C to determine at what temperatures thermal events would occur and how much energy would be released. Fig. 10 shows the DSC profiles for the cathode and anode of fully charged LTO/LMO and G/LMO cells (cells charged to top voltage and disassembled, which corresponds to a charged cathode and discharged anode). For both cells, the DSC profile of the LMO cathode material was the same, with a single exothermal peak that has an onset temperature of 280 °C. The anodes of the two cells had significant differences in their thermal characteristics. The graphite had an initial exothermal onset at 100 °C, while the onset of the first exothermal peak for the LTO was not until 130 °C. Also, the total energy released by the graphite was much greater than the LTO. The thermal event that began at 100 °C was consistent with the decomposition products observed in the gases collected from graphite cells aged at 100 °C (Figs. 8 and 9). DSC and analysis of the gases generated by LTO/LMO and G/LMO cells indicate that LTO is more stable to thermal abuse than graphite, which makes this material a very promising anode material for safety purposes.

4. Conclusions

Electrochemical characterization of pouch cells comprised of LTO and graphite anodes with LMO cathodes demonstrated that LTO has improved cycle life, calendar life, and pulsing impedance relative to graphite. Analysis of gases from lithiated LTO and graphite electrodes held at an elevated temperature indicated that graphite generated degradation products while LTO remained stable, and also the onset of exothermal reactions occurred at higher temperatures for LTO. These results demonstrate that LTO has advantages in safety and cycle life when compared to graphite, in particular when paired with LMO cathodes. So far, the safety, calendar life, and pulsing characteristics of a LTO/LMO cell make it attractive for HEVs and all battery power applications.

Acknowledgments

This research was funded by U.S. Department of Energy, FreedomCAR and Vehicle Technologies Office. Argonne National Laboratory is operated for the U.S. Department of Energy by UChicago Argonne, LLC, under contract DE-AC0Z-06CH11357.

References

[1] B. Scrosati, J. Garche, J. Power Sources 195 (2010) 2419.
[2] J.-M. Tarascon, M. Armand, Nature 414 (2001) 359.
[3] T.-F. Yi, L.-J. Jiang, J. Shu, C.-B. Yue, R.-S. Zhu, H.-B. Qiao, J. Phys. Chem. Sol. 71 (2010) 1236.
[4] K. Amine, I. Belharouak, Z. Chen, T. Tran, H. Yumoto, N. Ota, S.-T. Myung, Y.-K. Sun, Adv. Mater. 22 (2010) 3052.
[5] E. Ferg, R.J. Gummow, A. de Kock, M.M. Thackeray, J. Electrochem. Soc. 141 (1994) L147.
[6] M.M. Thackeray, J. Electrochem. Soc. 142 (1995) 2558.
[7] F. Bertaut, A. Durif, C. R. Hebd. Seances Acad. Sci. 236 (1953) 212.

[8] A. Deschanvres, B. Raveau, Z. Sekkal, Mater. Res. Bull. 6 (1971) 699.
[9] M.S. Whittingham, Prog. Solid State Chem. 12 (1978) 41.
[10] D.W. Murphy, R.J. Cava, S.M. Zahurak, A. Santora, Solid State Ionics 9 (1983) 413.
[11] K.M. Colbow, J.R. Dahn, R.R. Haering, J. Power Sources 26 (1989) 397.
[12] E. Rossen, J.N. Reimers, J.R. Dahn, Solid State Ionics 62 (1993) 53.
[13] T. Ohzuku, A. Aeda, Solid State Ionics 69 (1994) 201.
[14] T. Ohzuku, A. Aeda, N. Yamamoto, J. Electrochem. Soc. 142 (1995) 1431.
[15] D. Peramunage, K.M. Abraham, J. Electrochem. Soc. 145 (1998) 2609.
[16] A.N. Jansen, A.J. Kaihan, K.D. Kepler, P.A. Nelson, K. Amine, D.W. Dees, D.R. Vissers, M.M. Thackeray, J. Power Sources 81 (1999) 273.
[17] L. Aldon, P. Kubiak, M. Womes, J.C. Jumas, J. Olivier-Fourcade, J.L. Tirado, J.I. Corredor, C.P. Vicente, Chem. Mater. 16 (2004) 5721.
[18] D.H. Kim, Y.S. Ahn, J. Kim, Electrochem. Commun. 7 (2005) 1340.
[19] S. Scharner, W. Weppner, P. Schmid-Beurmann, J. Electrochem. Soc. 146 (1999) 857.
[20] S. Panero, P. Reale, F. Ronci, V. R.A., B. Scrosati, Ionics 6 (2000) 461.
[21] K. Amine, J. Liu, S. Kang, I. Belharouak, Y. Hyung, D.R. Vissers, G. Henricksen, J. Power Sources 129 (2004) 14.
[22] S.-H. Park, S.-H. Kang, I. Belharouak, Y.-K. Sun, K. Amine, J. Power Sources 177 (2008) 177.
[23] A. Mosbah, A. Verbaere, M. Tournoux, Mater. Res. Bull. 18 (1983) 1375.
[24] A. Lewandowski, A. Swiderska-Mocek, I. Acznik, Electrochim. Acta 55 (2010) 1990.
[25] DOE, PNGV battery test manual, DOE/ID-10597, 2001.
[26] I. Belharouak, Y.-K. Sun, W. Lu, K. Amine, J. Electrochem. Soc. 154 (2007) A1083.